Supporting Information

Synthesis and Characterization of Plasmonic Resonant Guided Wave Networks

Stanley P. Burgos[1,2,‡], *Ho W. Lee*[1,2,‡], *Eyal Feigenbaum*[1], *Ryan M. Briggs*[1], *and Harry A. Atwater*[1,2,†]

[1]Thomas J. Watson Laboratories of Applied Physics, California Institute of Technology, United States

[2]Kavli Nanoscience Institute, California Institute of Technology, United States

†Corresponding author e-mail: haa@caltech.edu

‡Equal author contribution

Keywords

Plasmonics, nanocircuits, resonant structures, power splitters, silicon photonics, logic device

1. Coupling Efficiency

Here, we investigate the coupling efficiencies associated in going from the photonic Si-ridge waveguide mode to the subwavelength CPP mode.[1, 2] Previous work has focused on coupling to the SPP mode of various structures, including DLSPP[3, 4], v-groove mode structures[5-8], and hybrid plasmonic-photonic modes[9-14]. As seen from the simulated mode patterns of v-groove CPP mode and Si-ridge waveguide mode in Fig. 1c and Fig. 1e in the main text, the CPP mode is ~1/5 the transverse size of the Si-ridge TE mode, so that we heuristically expect to have coupling efficiencies on this order.

However, due to fabrication imperfections, we find that the separation between the v-groove and Si-ridge waveguide is nonzero, and this reduces the coupling efficiency to a value smaller than their modal volume ratios. The coupling efficiency into the v-groove plasmonic waveguide mode will depend on the number of accessible modes that couple light from the Si-ridge to the CPP waveguide or to free space. Since we are coupling through a volume of free space, there is a large number of freespace modes that contribute to the coupling, making this calculation difficult to do analytically. Thus we have performed coupling efficiency calculations using full-wave finite-difference time domain simulations in which we launch light from a Si-ridge waveguide aligned to a v-groove waveguide separated by different distances and vertical offsets relative to their top surfaces (Fig. 1c-e in main text). The coupling efficiency is calculated by monitoring the power transmitted into the v-groove waveguide when excited by the TE Si-ridge mode at 1520 nm

As shown in the results in Fig. S1, we get a maximum coupling efficiency of ~14% at an offset of ~ −100 nm for a zero separation, which is only slightly lower than expected based on their modal volumes alone. However, this efficiency quickly drops as the separation is increased, going down to < 10% for 500 nm separation, and < 5% for 1000 nm separation. From NSOM measurements at 1520 nm, we measured a coupling efficiency of ~ 8%, consistent with FDTD calculated values for the geometries (Fig. S1, green dotted). We also measured the wavelength dependent coupling efficiencies by varying the excitation wavelength between 1490-1520 nm and repeating the power coupling calculation for the resulting NSOM images. The resulting data are shown in Fig S1, demonstrating coupling efficiencies in the 7-8% range.

To increase the coupling efficiency , we introduced a taper to the plasmonic v-groove waveguide (Fig. S2a).[1, 15] This figure (together with Fig. S1) clearly shows that the nanotaper indeed significantly increases the coupling coefficient and that high efficiency can be achieved with careful design of the taper geometries. The resulting transmission data is shown in Fig. S2a, from which we can see that with the introduction of taper with short taper length (with zero separation), we can obtain a maximum coupling efficiency of ~40%, almost independent of taper width. However the efficiency also drops as the separation is increased, shown in Fig. S2b going down to ~ 10% for 500 nm separation. From FIB cross-sections of the fabricated devices, we observed that the waveguides are separated by ~ 200 nm and offset

by ~ -50 nm, with taper dimension of dx = 250 nm, dy = 850 nm, thus placing our devices in the 20 % theoretical range for 1520 nm light, which is consistent with the value measured from the NSOM measurement (22.5 %, Fig. S2b, green dotted data).

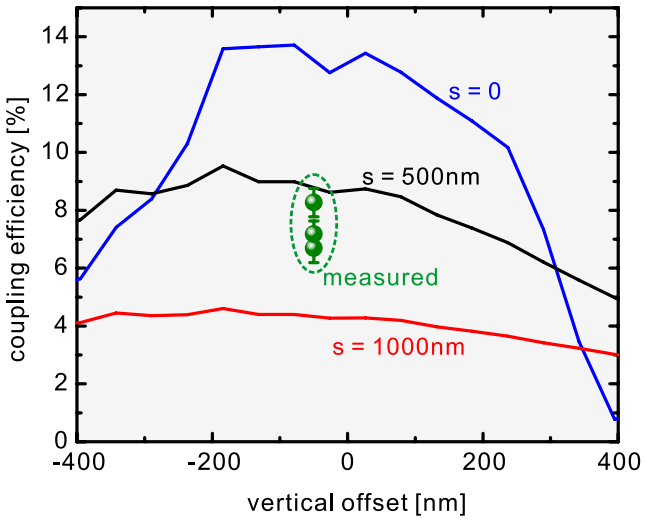

Figure. S1: Coupling efficiency as a function of waveguide position at λ_0 = 1520 nm. Horizontal axis corresponds to vertical offset between Si-ridge and v-groove waveguides relative to their surface tops. The three colored curves correspond to three different waveguide separations, with the blue corresponding to zero separation, black to 500 nm separation, and red to 1000 nm separation. The green dotted data corresponds to coupling efficiencies extracted from NSOM measurements for wavelengths λ_0 = 1500, 1510, and 1520 nm.

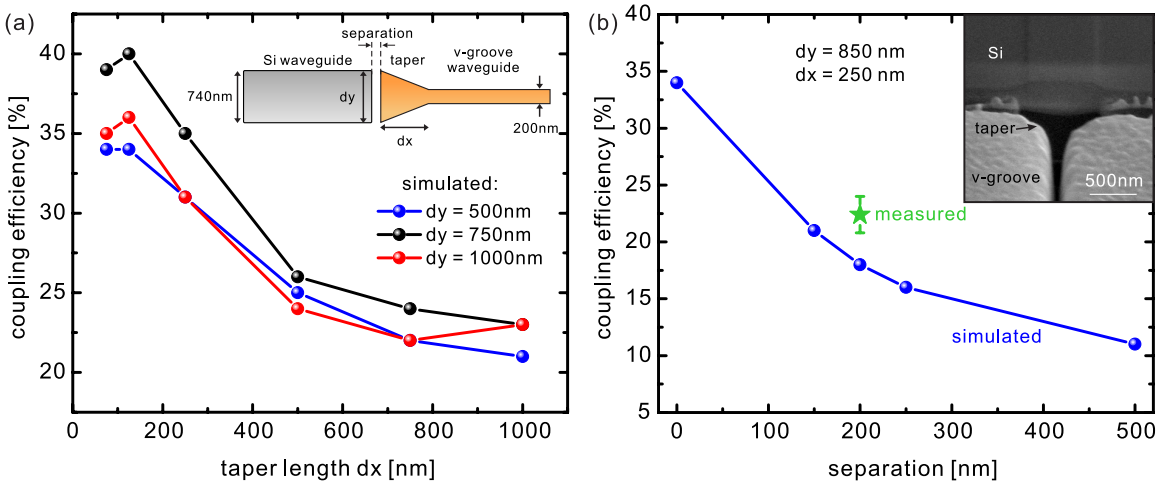

Figure S2: (a) Coupling efficiency as a function of taper length (dx) and width (dy) at λ_0 = 1520 nm (with zero separation). (b) Coupling efficiency as a function of separation for dx and dy of 850 nm and 250nm, respectively. The green data points correspond to coupling efficiencies extracted from NSOM measurements for wavelengths of λ_0 = 1520 nm.

2. Propagation of CPP and SPP at the x-junction

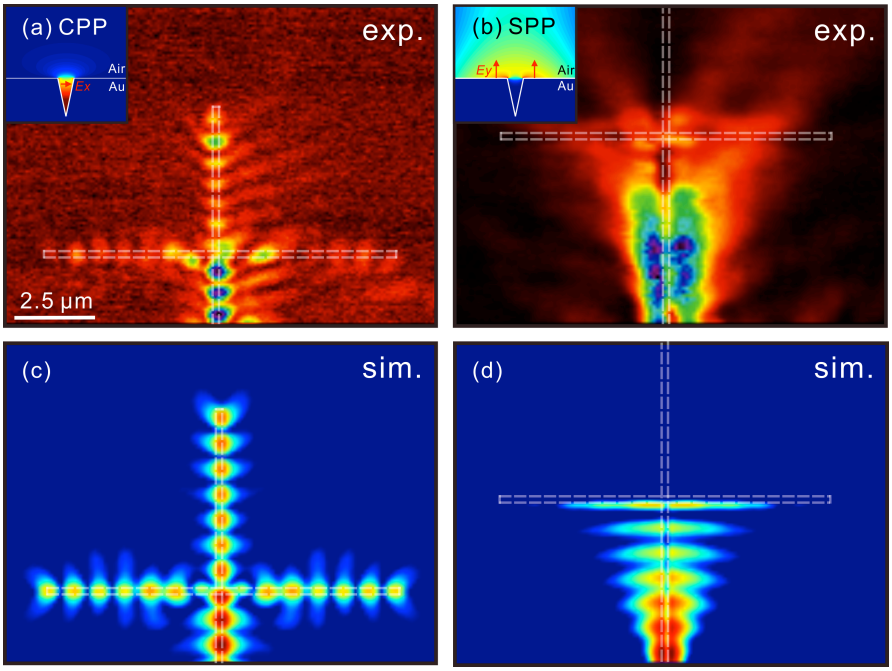

Figure. S3: NSOM image taken at λ_0 = 1520 nm of x-junction for (a) CPP and (b) SPP modes (the dashed lines indicate the location of the x-junction. Inset: simulated mode profiles of CPP and SPP modes. Corresponding simulated responses shown in (c) and (d), respectively.

To investigate the power splitting properties of the highly confined CPP mode and less confined SPP mode, these two modes were selectively excited (with the appropriate excitation angles) and the resulting near-field profiles at the x-junction were measured, as shown in Fig. S3a, b. It is clear from the figures that the CPP mode is split at the x-junction while the SPP mode is simply reflected. This can be explained from mode profile where the SPP mode is confined mainly on the top surface of the channel, resulting in a reflection of propagation due to the discontinuity of the surface at the x-junction. The simulated optical responses of the structures are shown in Figs. S3c, d, respectively, with both results in good agreement of each other. These results further suggest the uniqueness of the highly confined CPP mode for developing unltracompact plasmonic nanocircuit where sharp bends and power splitting junctions are required.

3. Silicon dielectric waveguide modes and dielectric x-junction splitter

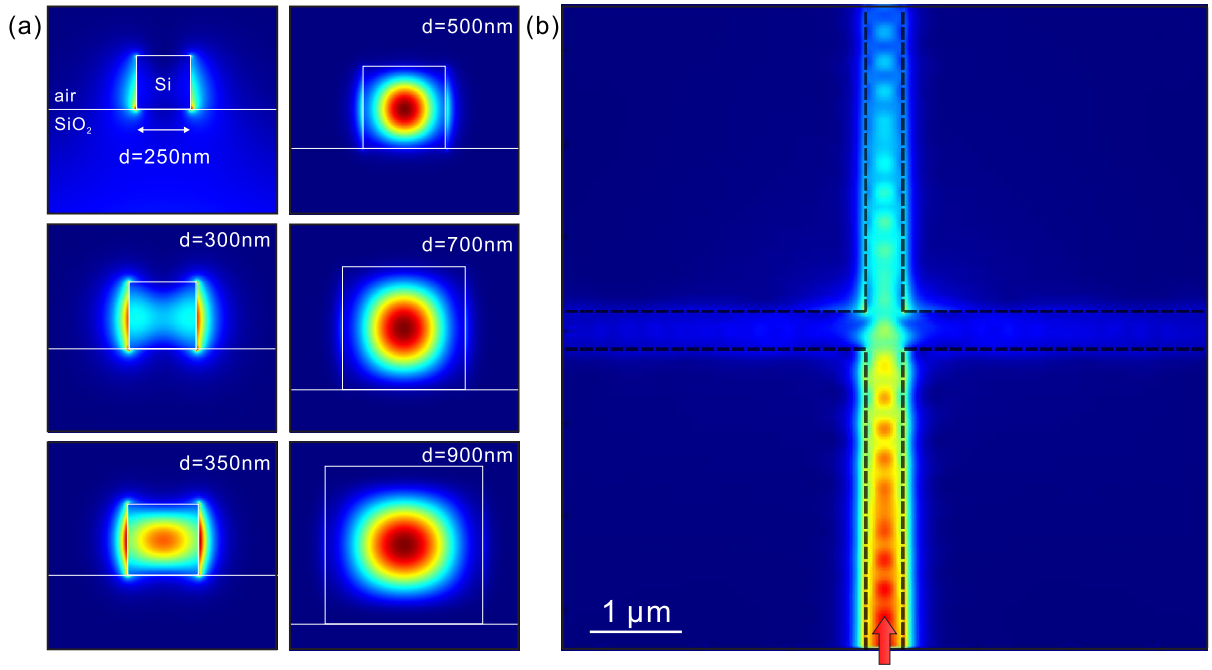

Figure. S4: (a) Simulated mode profiles of rectangular Si-waveguide with different dimension (with SiO_2 substrate). (b) Simulated responses of the propagating silicon photonic mode at dielectric x-junction.

The mode profiles of the rectangular silicon photonic waveguide with different dimensions are simulated using finite element method and the results are shown in Fig. S4a. As seen from the figure, the silicon dielectric mode extends out to the waveguide with the dimension below ~ 700nm, thus increasing the actual transverse mode profile. In addition, the propagation of the silicon dielectric mode with dimension of 350nm x 900nm are simulated with FDTD calculations. As shown in Fig. S4b, the propagating mode does not split to the side efficiently, instead most of the energy are propagated into the forward direction. Comparing this figure and Fig. S3c, it is clear that only the highly confined v-groove CPP mode is the only possible mode to be used as an efficient 4-way equal power splitter for ultracompact optical network design and development.

4. Calculation of splitting coefficients of x-junction

To calculate the back-reflected power in the power splitter we note that the length from the Si-slot/v-groove waveguide junction to the v-groove waveguide x-junction is only 7.5 microns, which is on the order of the propagation length of the v-groove waveguide, which is ~9 microns, as described in the propagation length section. Thus, the round-trip of the transmitted wave from the Si-slot/v-groove waveguide junction to the v-groove waveguide x-junction and back to the Si-slot/v-groove waveguide junction is ~15 microns, which is larger than the propagation length of the v-groove waveguide mode. For example, if the x-junction produced a perfect back-reflection, that means that only $e^{\frac{-15\mu m}{9\mu m}}$, =19% would reach the Si-slot/v-groove waveguide junction after being reflected by it. Furthermore, since we know that the x-junction is not perfect reflector, but that it only reflects ~25% of the incident power based on simulations, we get that only 25%×19%=4.5% is actually reaching the Si-slot/v-groove waveguide junction after the wave is reflected by the x-junction. Thus, ignoring the small amount of power that does reach the Si-slot/v-groove waveguide junction after it is reflected from the x-junction, we can use the following expression,

$$I_b(z) = \Psi_b \Psi_b^* = C^2\{1 + b^2 + 2b\cos[2\,k_{vgroove}(L - z) + \phi_b]\} \qquad (1)$$

In this case, C^2 is gives a DC offset in the intensity profile, corresponding to the amplitude squared of the incident wave onto the x-junction, which is the amount of light that transmitted into the v-groove channel. But this is no longer the variable of interest, we are interested in the variable *b*, which is related to the amplitude of the cosine function, which tells us how much of the incident wave is back-reflected in the power splitter. Aside from *L*, which is the arm length of the x-junction, $k_{v\text{-}groove}$ and ϕ_b are free fit parameters of the intensity function profile, which do not impact the *b*-coefficient, which is what we are after. Thus, by fitting the NSOM intensity profile in the back-reflected arm to Eqn. 1, we can extract the amplitude of the back-reflected coefficient of the x-junction.

5. Logical device with seven output ports

To demonstrate the potential of ultracompact logical devices using a 2x2 resonator, we numerically modeled the output intensity of all the output ports of the 2x2 device (ports 1-7 with port 8 as an input). Note that ports 3 and 4 are the same as ports A and B in Fig. 4 in the main text. As shown in Fig. S5, the output intensities of the seven ports vary with the input wavelength due to the complex closed loop resonances that arise within the resonator. The intensities of the output are normalized with the highest intensity port (port 1) at a wavelength of 1670 nm. By defining the threshold intensity (0.29 in this case), the resulting different on/off combinations for each port is outlined in Table S1, demonstrating a complex wavelength dependent logical device. It should be noted that by proper engineering the geometry of the device, such as the resonator and v-groove dimensions,[16, 17] a fully functional 2x2 logical device with 128 on/off combinations can be realized; however, this work is out of the scope of the present study.

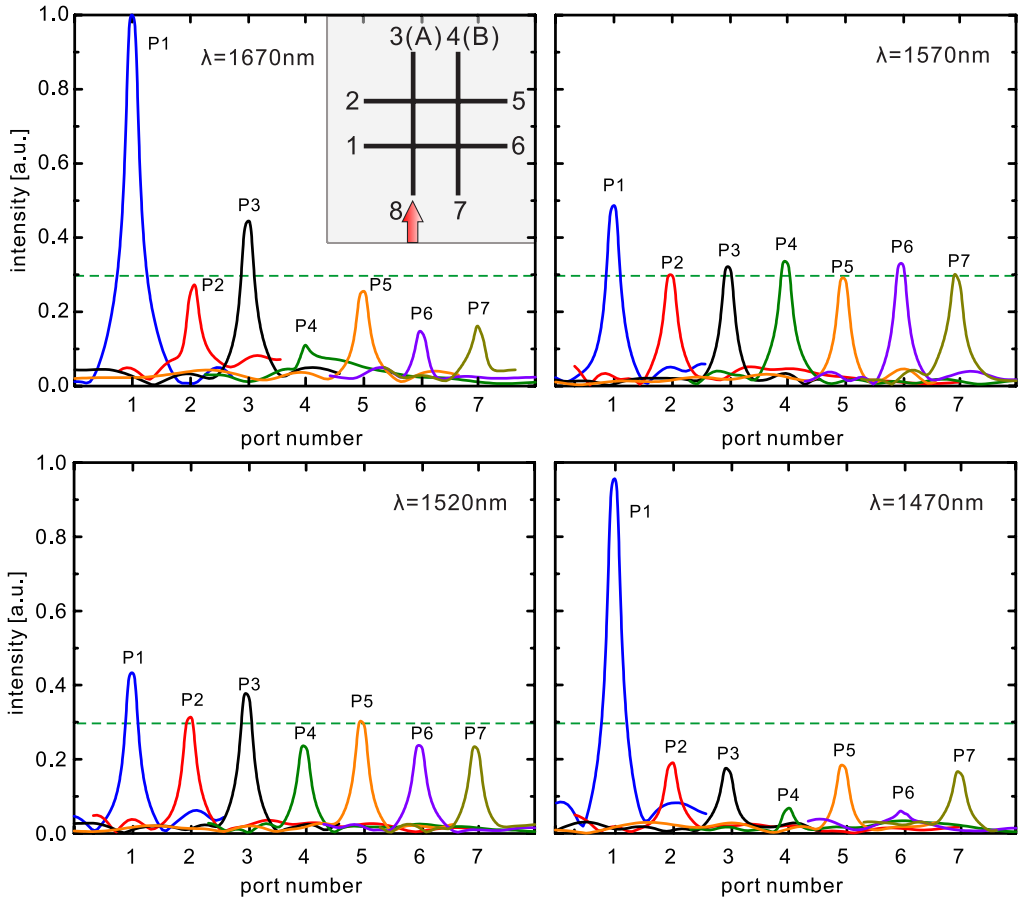

Figure. S5: 2x2 logical device with 7 output ports with different on/off configurations depending on the wavelength of excitation light. Threshold intensity is set to 0.29.

	Port 1	Port 2	Port 3	Port 4	Port 5	Port 6	Port 7
1670nm	1	0	1	0	0	0	0
1570nm	1	1	1	1	0	1	1
1520nm	1	1	1	0	1	0	0
1470nm	1	0	0	0	0	0	0

Table. S1: ON/OFF configurations of the 2x2 devices for all the seven output ports at different wavelength.

Reference:

(1) Veronis, G.; Fan, S. *Opt. Express* **2007**, 15, 1211–1221.

(2) Emboras, A.; Briggs, R. M.; Najar, A.; Nambiar, S.; Delacour, C.; Grosse, P.; Augendre, E.; Fedeli, J. M.; de Salvo, B.; Atwater, H. A.; Lamaestre, R. E. *Appl. Phys. Lett.* **2012**, 101, 251117.

(3) Briggs, R. M; Grandidier, J.; Burgos, S. P.; Feigenbaum, E.; and Atwater, H. A. *Nano Lett.* **2010**, 10, 4851–4857.

(4) Song, Y.; Wang, J.; Yan, M.; Qiu, M. *J. Opt.* **2011**, 13, 075002.

(5) Bozhevolnyi, S. I.; Volkov, V. S.; Devaux, E.; Laluet, J. Y.; Ebbesen, T. W. *Nature* **2006**, 440, 508–511.

(6) Bozhevolnyi, S. I.; Volkov, V. S.; Devaux, E.; Ebbesen, T. W. *Phys. Rev. Lett.* **2005**, 95, 046802.

(7) Volkov, V. S.; Bozhevolnyi, S. I.; Devaux, E.; Ebbesen, T. W. *Appl. Phys. Lett.* **2006**, 89, 143108.

(8) Zenin, V. A.; Volkov, V. S.; Han, Z.; Bozhevolnyi, S. I.; Devaux, E.; Ebbesen, T. W. *J. Opt. Soc. Am. B* **2011**, 28, 1596-1602.

(9) Shi, P.; Zhou, G.; Chau, F. S. *J. Opt. Soc. Am. B* **2013**, 30, 1426–1431.

(10) Nikolajsen, T.; Leosson, K.; Salakhutdinov, I.; Bozhevolnyi, S. I. *Appl. Phys. Lett.* **2003**, 82, 668–670.

(11) Zhu, S.; Liow, T. Y.; Lo, G. Q.; Kwong, D. L. *Opt. Express* **2011**, 19, 8888-8902.

(12) Sorger, V. J.; Lanzillotti-Kimura, N. D.; Ma, R. M.; Zhang, X. *Nanophotonic* **2012**, 1, 17-22.

(13) Lou, F.; Wang, Z.; Dai, D.; Thylen, L.; Wosinski, L. *Appl. Phys. Lett.* **2012**, 100, 241105.

(14) Lau, B.; Swillam, M. A.; Helmy, A. S. *Opt. Express* **2010**, 18, 27048–27059.

(15) Kocabaşo S. E.; Veronis, G.; Miller, D. A. B.; Fan, S. *Phys. Rev. B* **2009**, 79, 035120.

(16) Feigenbaum, E.; Atwater, H. A. *Phys. Rev. Lett.* **2010**, 104, 147402.

(17) Feigenbaum, E.; Burgos, S. P.; Atwater, H. A. *Opt. Express* **2010**, 18, 25584–25595.